Biomaterials Advances 165 (2024) 214024

Contents lists available at ScienceDirect

Biomaterials Advances

journal homepage: www.journals.elsevier.com/materials-science-and-engineering-c

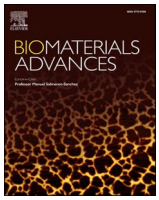

Defining the immunological compatibility of graphene oxide-loaded PLGA scaffolds for biomedical applications

Andrea Papait [a,b,*,1], Giordano Perini [b,c,1], Valentina Palmieri [b,c,e], Anna Cargnoni [d], Elsa Vertua [d], Anna Pasotti [d], Enrico Rosa [b,c], Marco De Spirito [a,b], Antonietta Rosa Silini [d], Massimiliano Papi [b,c], Ornella Parolini [a,b]

[a] Dipartimento di Scienze della Vita e Sanità Pubblica, Università Cattolica del Sacro Cuore, Largo Francesco Vito 1, 00168 Rome, Italy
[b] Fondazione Policlinico Universitario A. Gemelli IRCSS, 00168 Rome, Italy
[c] Dipartimento di Neuroscienze, Università Cattolica del Sacro Cuore, Largo Francesco Vito 1, 00168 Rome, Italy
[d] Centro di Ricerche Eugenia Menni, Fondazione Poliambulanza Istituto Ospedaliero, 25124 Brescia, Italy
[e] Istituto dei Sistemi Complessi, CNR, via dei Taurini 19, 00185 Rome, Italy

ARTICLE INFO

Keywords:
Graphene oxide
3D printed scaffolds
Immune response
Toxicity
Adaptive immunity
Innate immunity
Differentiation

ABSTRACT

Graphene oxide (GO), a carbon-based nanomaterial, presents significant potential across biomedical fields such as bioimaging, drug delivery, biosensors, and phototherapy. This study examines the effects of integrating GO into poly(lactic-*co*-glycolic acid) (PLGA) scaffolds on human immune cell function. Our results demonstrate that high concentrations of GO reduce the viability of peripheral blood mononuclear cells (PBMCs) following stimulation with anti-CD3 antibody. This reduction extends to T lymphocyte activation, evident from the diminished proliferative response to T cell receptor engagement and impaired differentiation into T helper subsets and regulatory T cells. Interestingly, although GO induces a minimal response in resting monocytes, but it significantly affects both the viability and the differentiation potential of monocytes induced to mature toward M1 pro-inflammatory and M2-like immunoregulatory macrophages. This study seeks to address a critical gap by investigating the in vitro immunomodulatory effects of PLGA scaffolds incorporating various concentrations of GO on primary immune cells, specifically PBMCs isolated from healthy donors. Our findings emphasize the need to optimize the GO to PLGA ratios and scaffold design to advance PLGA-GO-based biomedical applications.

Statement of significance: Graphene oxide (GO) holds immense promise for biomedical applications due to its unique properties. However, concerns regarding its potential to trigger adverse immune responses remain. This study addresses this critical gap by investigating the in vitro immunomodulatory effects of PLGA scaffolds incorporating increasing GO concentrations on human peripheral blood mononuclear cells (PBMCs). By elucidating the impact on cell viability, T cell proliferation and differentiation, and the maturation/polarization of antigen-presenting cells, this work offers valuable insights for designing safe and immunologically compatible GO-based biomaterials for future clinical translation.

1. Introduction

Graphene based biomaterials exhibit wide possibilities in the biomedical field, spanning from bioimaging, drug delivery, biosensors, and phototherapy. Among these, graphene oxide (GO) stands out as a pivotal carbon-based nanomaterial with extensive biomedical potential [1]. Leveraging its chemical properties, GO offers different sites for functionalization, by anchoring genes and drug molecules. One notable application involves enhancing tumor therapy efficiency by linking hydrophobic camptothecin (CPT) analogues [2]. Furthermore, GO is used as a vehicle for thermotherapy, generating heat through near-infrared irradiation to mediate cancer cell death [3]. Nevertheless, with the emerging health applications of GO, concerns have arisen regarding potential impacts on cellular functionality and the risk of triggering adverse immune system reactions following administration [3]. The encapsulation of dispersed nanoparticles within biocompatible

* Corresponding author at: Dipartimento di Scienze della Vita e Sanità Pubblica, Università Cattolica del Sacro Cuore, Largo Francesco Vito 1, 00168 Rome, Italy.
E-mail address: andrea.papait@unicatt.it (A. Papait).
[1] Equal contribution.

https://doi.org/10.1016/j.bioadv.2024.214024
Received 13 May 2024; Received in revised form 9 August 2024; Accepted 30 August 2024
Available online 31 August 2024

matrices has garnered attention both to curb biotoxicity and prolong residence time, as well as to protect from degradation [4,5].

Within this context, we propose the utilization of Poly(lactic-*co*-glycolic acid) (PLGA), an FDA and EMA approved biodegradable polyester copolymer, as a matrix material for incorporating GO. Saturated poly(α-hydroxy esters), such as poly(lactic acid) (PLA), poly(glycolic acid) (PGA), and their copolymer poly(lactic-co-glycolide) (PLGA), are extensively used in creating biodegradable synthetic polymers for three-dimensional (3D) scaffolds in tissue engineering applications with extensive applications across various fields, including dentistry, orthopedics, and wound dressing [6–8].

By combining the ratios of polylactic acid (PL) and glycolic acid (GA), PLGA enables precise tuning of mechanical properties, including tensile strength and flexibility, to meet specific clinical demands [9]. Increasing the GA content enhances scaffold strength, while higher PL content improves flexibility, enabling customized designs for diverse clinical applications. Manipulating GA levels can accelerate scaffold degradation, whereas adjusting PL content can prolong it, resulting in tailored degradation and resorption kinetics [10,11]. This polymer exhibits excellent biocompatibility characteristics [12,13], largely due to the fact that PLGA polymers are readily degraded by esterase enzymes. This degradation process results in the formation of lactic and glycolic acids, which are metabolized via the Krebs cycle and eliminated as CO2 and water through respiration, feces, and urine [14,15]. Furthermore, when used at low concentrations, there have been no reports of polymer accumulation in human organs. However, in certain instances, failure to eliminate these degradation byproducts can lead to the in-situ accumulation of acidic products (lactic and glycolic acids), which may become hazardous by altering biological responses when they accumulate at high local concentrations [16]. However, it has been reported that PLGA induces a minimal inflammatory response, exhibits no apparent immunostimulatory properties, and may even possess immunosuppressive effects [17–19].

This characteristic becomes even more crucial for a biomaterial considering that, upon implantation, biomaterials initiate interactions with host tissues, eliciting responses from innate immune cells such as neutrophils, macrophages, and dendritic cells (DCs). These cells constitute the body's initial defense against foreign elements and play a crucial role in maintaining tissue homeostasis, thereby influencing healing and repair processes [20]. Various studies have emphasized the capacity of GO-based nanosheets to induce stress, incite immune responses, and trigger the death of immune cells, including T lymphocytes, macrophages, and dendritic cells [21,22]. For example, GO has been associated with the formation of neutrophil extracellular traps [23,24]. Furthermore, GO can act as a positive modulator by promoting DCs maturation and enhancing their secretion of cytokines through the activation of multiple toll-like receptor (TLR) pathways, while showing low toxicity. Additionally, this GO–PEG–PEI combination can serve as an effective antigen carrier for transporting antigens into dendritic cells [25]. Conversely, GO has demonstrated the potential to inhibit the antigen presentation capabilities of dendritic cells, consequently reducing the activation of T lymphocytes [26].

In this study, we analyzed the in vitro immune responses triggered by PLGA scaffolds loaded with increasing concentrations of GO by employing peripheral blood mononuclear cells (PBMCs) isolated from healthy donors. Our investigation highlights the impact of PLGA-GO constructs on immune cell viability, on the ability of T cells to proliferate and differentiate in response to external stimuli, as well as on the maturation and polarization of antigen-presenting cells (DCs and macrophages) in terms of acquisition of pro-inflammatory or immunoregulatory markers.

2. Materials and methods

2.1. Ethics statements

The collection of human peripheral blood mononuclear cells (PBMCs) from healthy donors for research purposes was approved by the ethical local committee "Comitato Etico Provinciale di Brescia" Italy (NP 3968, July 2, 2020).

2.2. PLGA-graphene oxide (GO) scaffold 3D-printing and characterization

3D printing of PLGA-GO scaffolds was conducted using a BIO X 3D bioprinter (Cellink, Gothenburg, Sweden). Prior to printing, spectroscopic and microscopic characterization of GO (Graphenea, Cambridge, MA, United States) was performed. Spectroscopic analysis involved dynamic light scattering (DLS), zeta-potential and absorbance measurement. DLS and zeta-potential analysis were conducted using a Zetasizer Nano S from Malvern Instruments (Malvern, Worcestershire, United Kingdom) equipped with a 4 mW He—Ne laser (633 nm). GO samples were diluted at a final concentration of 0.1 mg/mL in double-distilled water (Milli-Q). Measurements were undertaken at a constant angle of 173° relative to the incident beam. Absorbance measurement was carried out using a Cytation 3 Cell Imaging Multi-Mode Reader (Biotek, California, United States). For this purpose, GO was diluted to a concentration of 0.1 mg/mL in double-distilled water (Milli-Q). Microscopic characterization was carried out using atomic force microscopy (AFM) with a NanoWizard II (JPK Instruments, Berlin, Germany) [27]. Silicon cantilevers with high aspect-ratio conical silicon tips (CSC36 Mikro-Masch, Sofia, Macedonia), featuring an end radius of approximately 10 nm, a half conical angle of 20°, and a spring constant of 0.6 N/m, were employed for imaging. Small scan areas (5 × 5 μm) were examined, and lateral size was determined using JPK Data Processing software (JPK Instruments, Berlin, Germany). Following GO characterization, a mixture of PLGA flakes (Rimless Industry, Changchun, Jilin, China) and GO was prepared in dichloromethane (Carlo Erba, Milan, Italy), with a fixed amount of PLGA and varying GO content ranging from 0 to 5 % *w*/w. The mixture was agitated overnight and subsequently air dried. The resulting film was cut into small pieces and transferred a thermoplastic printhead (Cellink, Gothenburg, Sweden), which is able to heatup to 250 °C. Scaffold structures were designed using computer-aided design (CAD) software Rhinoceros (Robert McNeel & Associates, Seattle, United States). Printing of PLGA-GO scaffolds was accomplished via an extrusion-based technique, with printhead temperature set at 185 °C and printing bed temperature at 65 °C. Extrusion pressure was maintained at 40 kPa, with a preflow of 20 ms and a printing speed of 22 mm/s. Post-printing, Fourier-transform infrared spectroscopy (FTIR) was performed using an ALPHA II compact FTIR spectrometer (Bruker) to assess the surface chemical composition of scaffolds. Samples were directly placed onto the crystal, and spectra were recorded within the wave number range of 4000–550 cm^{-1}. To verify possible toxic effects induced by reactive oxygen species (ROS) release from discs, the ROS-ID detection kit was used (Enzo Life Sciences). The kit allows for the assessment of comparative levels of total ROS, while also enabling the determination of superoxide production. The kit comprises two major components: the Oxidative Stress Detection Reagent (Green) for ROS detection and the Superoxide Detection Reagent (Orange). The green probe reacts directly with a broad spectrum of reactive species, yielding a green fluorescent product indicative of cellular production of various ROS types. In contrast, the orange probe, a cell-permeable superoxide detection dye, specifically reacts with superoxide, generating an orange fluorescent product. In our study, we incubated PLGA-GO scaffolds in 48-well plates (Corning, New York, United States) in the Detection Solution for 1 h. After incubation, fluorescence intensity in the supernatant was recorded with a Cytation 3 Cell Imaging Multi-Mode Reader (Biotek, California, United States) by

exciting at 490 nm and reading the emission at 525 nm (green probe) and by exciting at 550 nm and reading the emission at 620 nm (orange probe).

2.3. Cell apoptosis detection

For assessment of cell viability and apoptosis, FITC-Annexin V-propidium iodide (PI) kit was used following manufacturer instruction (BD Biosciences, Franklin Lakes, New Jersey, U.S). Following a 15-min incubation in darkness at room temperature, the samples underwent two washing steps with binding buffer. Subsequently, the cells were resuspended to a final volume of 200 μL for subsequent analysis.

The stained cells were analyzed with flow cytometry using a FACS Symphony A3system (BD Biosciences, Franklin Lakes, New Jersey, U.S.) within an hour of staining. The collected data was analyzed utilizing FlowJo version 10.7v software (BD Biosciences, Franklin Lakes, New Jersey, U.S.). Cells were distinguished in early apoptotic phase (Annextin V+/PI-), late apoptotic phase (Annextin V+/PI+) and necrotic phase (Annexin V-/PI+).

2.4. Analysis of PBMC proliferation in presence of graphene-functionalized scaffolds

To investigate the effects of graphene oxide (GO)-functionalized scaffolds, termed as PLGA-GO, on activated peripheral blood mononuclear cells (PBMCs), a systematic approach was employed. Human peripheral blood mononuclear cells (PBMCs) were obtained from heparinized whole blood samples through density gradient centrifugation, employing Histopaque 1077 (Sigma-Aldrich, St. Louis, MO, USA).

PBMCs were seeded at a density of 1 × 105 cells per well within a 96-well plate. Activation was achieved by treating PBMCs with 125 ng/mL of the anti-CD3 monoclonal antibody (Orthoclone OKT3, Janssen-Cilag, Cologno Monzese, Italy).

The activated PBMCs were then cultured for 3 days in RPMI 1640 medium (supplemented with 10 % heat-inactivated fetal bovine serum, 2 mM L-glutamine, and penicillin-streptomycin, all from Sigma-Aldrich, St. Louis, MO, USA). During the culture period, PBMCs were exposed to different experimental conditions, including the presence of a Poly-(lactic-*co*-glycolic acid) (PLGA) scaffolds (Rimless Industry, Changchun, Jilin, China) or PLGA scaffolds functionalized with varying percentages of graphene oxide (0.5 %, 1 %, 2 %, 5 %) (Rimless Industry, Changchun, Jilin, China) denoted as PLGA+GRAPH OX. Control conditions were activated PBMCs cultured alone or in presence of the PLGA scaffold alone. All experimental conditions, including controls, were performed in triplicate.

The assessment of PBMC proliferation was performed by the analysis of incorporated 5-ethynyl-2′-deoxyuridine (EdU), a technique previously described [28]. Briefly, on day 3 post-stimulation, PBMCs were exposed to 10 μM EdU (Life Technologies, Carlsbad, CA, USA). Following a subsequent 16 to 18-h incubation period, cells were harvested and EdU incorporation was quantified. This was performed by introducing 2.5 μM 3-azido-7-hydroxycoumarin (Jena Biosciences, Jena, Germany) in a buffer solution (composed of 100 mM Tris-HCl pH 8.0, 10 mM L-ascorbic acid, and 2 mM CuSO4) at room temperature for 30 min. The acquired cells were analyzed using a FACS Symphony A3 (BD Biosciences). The Flowjo v10.7 software was utilized to assess the percentage of EdU-positive proliferating cells, and E-Fluor 780 (Thermo Fisher, Waltham, Massachusetts, United States) staining was performed to exclude non-viable cells from the analysis.

2.5. Identification of T helper subpopulations and T regulatory cells using flow cytometry

Flow cytometry was employed to comprehensively investigate the impact of graphene oxide (GO)-functionalized scaffolds on T cell differentiation toward T helper (Th) subpopulations (Th1, Th2, Th17, Th1/Th17) and regulatory T cells (Tregs). The expression of specific cell surface markers and transcription factors that characterize the different T cell subsets was analyzed. Activated peripheral blood mononuclear cells (PBMCs) were *co*-cultured with or without Poly(lactic-*co*-glycolic acid) (PLGA) scaffold, either alone or functionalized with varying percentages of graphene oxide (0.5 %, 1 %, 2 %, 5 %). Following a 5-day co-culture period, the activated PBMCs were harvested and centrifuged at 300 *g* for 5 min. To exclude non-viable cells from analysis, viable dye *E*-Fluor 780 (Thermofisher) was employed. Flow cytometry analysis was conducted to identify specific T cell subsets. For this purpose, the following antibodies were used: CD3 (clone UCHT1), CD4 (clone VIT-4), CD45RA (clone HI100), CD196 (clone 11A9), CD183 (clone 1C6/CXCR3), CD25 (clone M-A25) from BD Biosciences, and CD194 (clone REA279) from Miltenyi. Following fixation and permeabilization with BD Cytofix/Cytoperm (BD Biosciences), intracellular staining for the transcription factor FoxP3 was performed. The anti-FoxP3 antibody (clone R16–715, BD Biosciences) was incubated with cells at 4 °C for 30 min in the dark. Acquisition of the samples was performed using the FACS Symphony A3 (BD Biosciences) flow cytometer, and subsequent analysis was conducted using Flowjo 10.7v (BD Biosciences) software. The gating strategy for identifying T helper subpopulations and Tregs was as follows. First, CD4 + CD45RA negative cells were gated to identify T effector cells. Within the T effector cell gate, Th subsets were identified: Th1: CD196-CD183+, Th17/Th1: CD196 + CD183+, and Th2: CD196-CD183-CD194+. Regulatory T cells (Tregs) were identified by gating on $CD25^{hi}FoxP3^{+}$ cells [28].

2.6. Analysis of monocyte differentiation toward antigen-presenting cells

To stimulate differentiation toward dendritic cells (mDCs), a total of 2.5×10^5 peripheral blood mononuclear cells (PBMCs) were cultured in 48-well plates for a duration of four days (Corning). This culture was conducted in the presence of 50 ng/mL recombinant human IL-4 (R&D Systems, Minneapolis, MN, USA) and 50 ng/mL granulocyte macrophage colony stimulating factor (GM-CSF, Miltenyi Biotec, Bergisch Gladbach, North Rhine-Westphalia, Germany) using 0.5 mL of RPMI 1640 complete medium (Sigma Aldrich). The process of complete maturation was achieved by the addition of 0.1 μg/mL lipopolysaccharide (LPS, Sigma Aldrich) for two days.

For the generation of monocyte-derived M1 macrophages, 5×10^5 PBMCs were cultured in 24-well plates for four days (Corning). This culture was conducted in the presence of 5 ng/mL GM-CSF (Miltenyi Biotec, Bergisch Gladbach, North Rhine-Westphalia, Germany) using 0.5 mL of RPMI 1640 complete medium (Sigma Aldrich). Full differentiation into M1 macrophages was achieved by treating the cells with 20 ng/mL interferon gamma (IFN-γ) for 1 h, followed by the administration of 0.1 μg/mL LPS (Sigma-Aldrich), and incubating for an additional two days.

To obtain M2-derived macrophages, 5×10^5 were cultured in 24-well plates at 37 °C in 1 mL RPMI complete medium containing 20 ng/mL M-CSF (Miltenyi Biotec, Bergisch Gladbach, North Rhine-Westphalia, Germany) for 4 or 5 days and subsequently supplemented with 20 ng/mL interleukin-4 (IL-4; Miltenyi Biotec, Bergisch Gladbach, North Rhine-Westphalia, Germany) for 1 h and then with 0.1 μg /mL LPS (Sigma-Aldrich) for 48 h.

The differentiation into M1 macrophages was evaluated through flow cytometry analysis. Live cells, distinguished by E-Fluor 780 staining, underwent analysis for the expression of a panel of surface markers. The gating strategy involved initially excluding CD3-negative cells and subsequently assessing the expression of CD11b (clone ICRF44) in the CD11b-positive population. Further examination included the evaluation of CD163 (clone GHI/61), CD209 (clone DCN46), CD197 (clone 3D12), CD86 (clone 2331 (FUN-1)), and CD14 (clone MP9) expressions. All antibodies were from BD Biosciences.

2.7. Statistical analysis

The data are represented as violin truncated plots with Tukey variations. The parameters were compared using one way or two-way analysis of variance (ANOVA). The normality of the distribution was assessed using a Q-Q probability plot and analytically evaluated through the Shapiro–Wilk test and the Kolmogorov–Smirnov test. Detailed statistical information for each experiment, including the median, quartiles, and sample size (n), is provided in the figure legends. Statistical analyses were conducted using Prism 9 (GraphPad Software, La Jolla, CA, USA). A p-value of <0.05 was considered statistically significant.

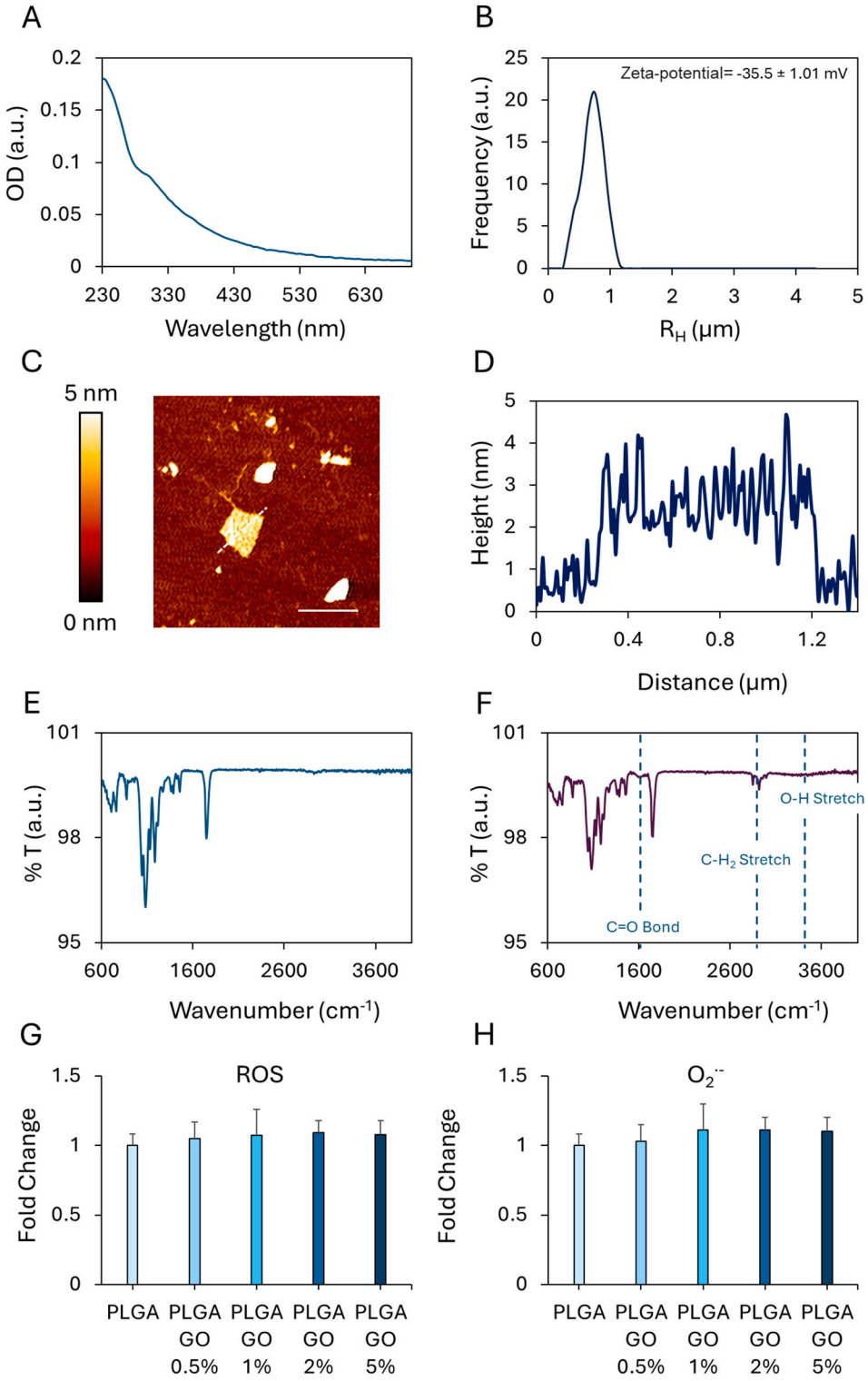

Fig. 1. Characterization of 3D-Printed Scaffolds. Absorbance spectrum of graphene oxide (GO) (A). Hydrodynamic radius and zeta-potential of graphene oxide in water (B). Atomic force microscopy (AFM) imaging (C) and lateral size (D) of GO. Scalebar 1 μm. Fourier-transform infrared spectra of PLGA (E) and PLGA-GO (F) scaffolds, showing the relative absorption peaks. Total reactive oxygen species (ROS) production of the 3D-printed scaffolds (G, H).

3. Results

3.1. 3D-printing and characterization of PLGA-GO scaffolds

Scaffolds were composed of PLGA and GO at different concentrations, ranging from 0 to 5 % *w*/w [29]. Prior to printing, GO was first characterized by spectroscopic and microscopic techniques. Absorption spectra revealed distinct peaks characteristic of GO at wavelengths ranging from 230 to 700 nm. The absorbance spectra showed a broad peak centered around 230 nm attributed to π-π* transitions of the aromatic C—C bonds, and a shoulder peak at around 300 nm indicative of n-π* transitions, as shown in Fig. 1A [30,31]. Dynamic light scattering (DLS) scattering and zeta-potential measurements of GO are reported in Fig. 1B. A hydrodynamic radius peaked at 742 nm and a surface net charge of – 35.5 mV were revealed for GO. The atomic force microscopy (AFM) images of GO (Fig. 1C) showed distinct features consistent with the expected morphology of GO sheets. The height analysis indicated a thickness of 0.8 nm for the GO sheets, consistent with previous reports [32]. The lateral size reported on Fig. 1D was around 800 nm, consistently with DLS data. After characterization of GO, PLGA-GO scaffolds were 3D printed via an extrusion-based technique. The amount of PLGA was fixed and GO varied from 0.5 to 5 % *w*/w. Fourier-transform infrared spectroscopy (FTIR) was employed for the validation of the chemical composition of the scaffolds (Fig. 1E, F). The spectra of both PLGA and PLGA-GO exhibited characteristic absorption peaks at 2990 and 2890 cm^{-1}, indicative of the C—H stretching of CH2 and –C–H– groups, respectively [33]. Additionally, both scaffolds displayed peaks at 1700 cm^{-1} (corresponding to the C═O stretching of the ester bond), and at 1000 cm^{-1} (corresponding to C—O stretching) [34]. Notably, the incorporation of GO into the 3D printed materials was confirmed in the PLGA-GO spectra, where a broad absorption peak spanning from 3600 to 3100 cm^{-1}, attributed to O—H stretching vibration, and a narrower peak at 1500 cm^{-1}, associated with the C═O bond, were observed. To perform a preliminary evaluation of the potential toxicity of 3D-printed scaffolds, we assessed the production of reactive oxygen species (ROS) in the culture medium [35]. For this purpose, we discriminated general ROS and superoxide through the use of two distinct probes: a green fluorescent dye for the detection of general ROS (Fig. 1G), such as hydrogen peroxide (H_2O_2), peroxynitrite ($ONOO^-$), hydroxyl radicals (OH•), nitric oxide (NO), and peroxy radical (ROO); an orange fluorescent probe (Fig. 1H), capable of detecting O2•-. We did not observe statistically significant substantial increase in the production of reactive oxygen species and superoxide following scaffold incubation with the probes.

3.2. Graphene oxide (GO) embedded in a PLGA matrix has minor effects on the viability of PBMCs

Before examining the influence of GO on immune cell functions, we investigated whether exposure to increasing concentrations of GO within a PLGA scaffold influenced the viability of unstimulated (Fig. 2A) and activated PBMCs (Fig. 1B). We employed a PI-AnnV assay to determine the proportion of viable (AnnV-PI-), early apoptotic (AnnV+ PI-), late apoptotic (AnnV+ PI+), and necrotic (AnnV- PI+) immune cells resulting from exposure to various GO concentrations. Our observations revealed that while in unstimulated PBMCs there were no discernible differences in viability regardless of the GO concentration (Fig. 1A), in stimulated PBMCs the higher GO concentrations (2 and 5 %) led to minimal decline in cell viability (Fig. 2B). No toxic effects were observed for the PLGA scaffold alone, both in unstimulated PBMCs and PBMCs stimulated with anti-CD3.

3.3. High concentrations of graphene oxide (GO) reduce the proliferation of stimulated PBMCs

In light of the minimal impact observed on viability of activated PBMC, we investigated at which concentration ranges GO can affect PBMC proliferation. The analysis of unstimulated PBMCs (Fig. 3A) indicates that neither the PLGA scaffold alone nor the addition of GO at increasing concentrations appear capable of inducing an immunogenic response. However, when examining the ability of PBMCs to respond to direct stimulation with anti-CD3 monoclonal antibodies, the PLGA scaffold alone slightly reduced the activation of PBMCs, though this effect was not statistically significant. Additionally, the presence of GO-conjugated PLGA scaffolds significantly inhibited PBMC proliferation upon stimulation with anti-CD3 mAbs in a concentration dependent manner reaching significance at the highest concentration tested (PLGA-GO 5 %) (Fig. 3B).

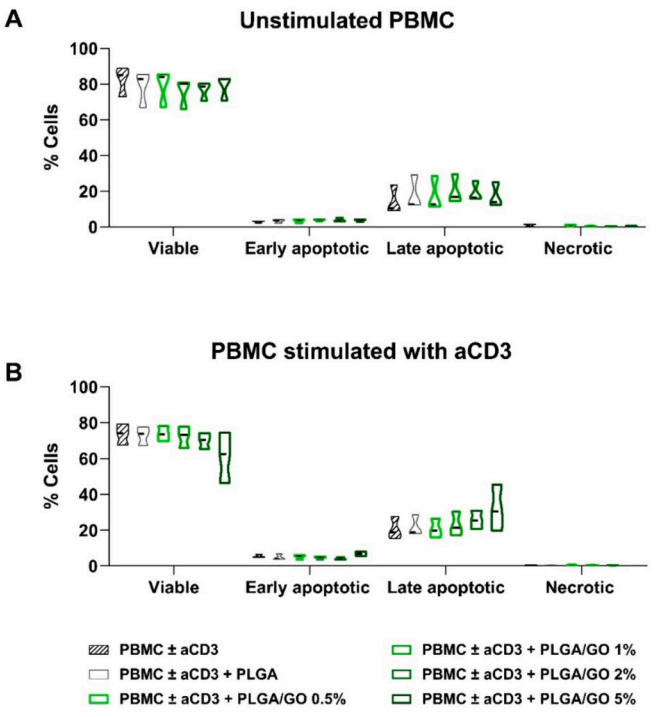

Fig. 2. Increasing concentrations of GO embedded in a PLGA matrix have a slight impact on the viability of PBMCs. Unstimulated (A) and anti-CD3 (aCD3) stimulated PBMCs (B) were cultured in the presence of PLGA scaffolds with different concentrations of graphene oxide (0.5, 1, 2 and 5 %) (GO). The control conditions are represented by PBMC cultured in absence of the scaffold (first line, in red), and by PBMC in the presence of the scaffold constituted by the PLGA matrix alone (second line, dark blue). Results are expressed as percentage of viable, early apoptotic, late apoptotic or necrotic cells. Results are displayed as violin plots showing median (thick line), 25th and 75th quartiles. $N = 3$ individual experiments. The data passed the Shapiro–Wilk test and the Kolmogorov–Smirnov normality test, thus exhibiting a normal distribution.

3.4. Graphene oxide (GO) impacts the differentiation of CD4+ T lymphocytes

Given that high concentrations of GO inhibited the proliferation of activated PBMCs, we investigated whether GO could influence the differentiation of CD4+ lymphocytes into various T helper (Th) subsets. While increasing concentrations of GO did not affect the expression of differentiation markers on resting CD4+ lymphocytes (Fig. 4A), they significantly affected the differentiation of activated PBMCs (Fig. 4B). More in detail, 1 % GO was able to reduce the differentiation of CD4+ T lymphocytes toward the inflammatory Th1 subset, and this effect reached statistical significance when 5 % GO was used (Fig. 4B). Conversely, the highest concentration of GO promoted differentiation toward the Th2 subset, with no significant differences observed in the polarization toward Th1/Th17 and Th17 subsets (Fig. 4B).

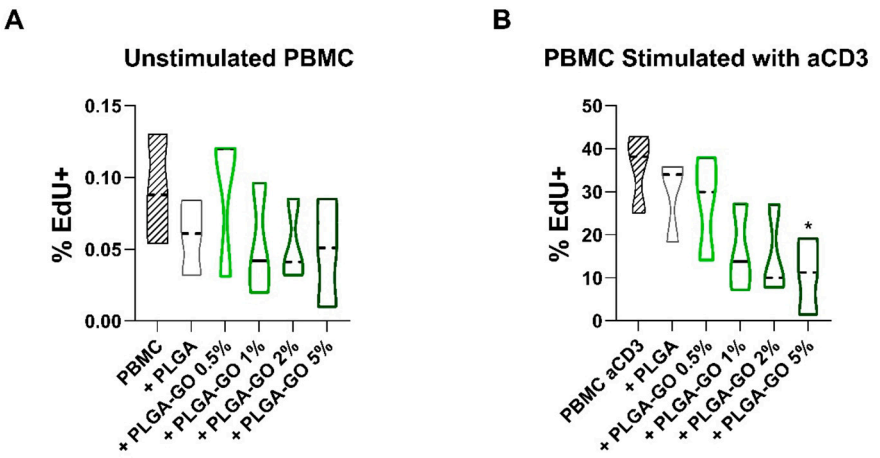

Fig. 3. Higher concentrations of GO embedded in a PLGA matrix reduce the proliferation of stimulated PBMCs. PBMC were stimulated with anti-CD3 mAb (aCD3) in the presence of PLGA scaffolds with different concentrations of graphene oxide (0.5, 1, 2 and 5 %), (GO) in comparison to the control condition in red in unstimulated (A) and antiCD3 stimulated PBMC, (B) Results are expressed as percentage of Edu positive proliferating cells. Results are displayed as violin plots showing median (thick line), 25th and 75th quartiles (*$p < 0.01$, ***$p < 0.001$ versus control (PBMC + anti-CD3)), A: $N = 3$; individual experiments. The data passed the Shapiro–Wilk test and the Kolmogorov–Smirnov normality test, thus exhibiting a normal distribution.

Furthermore, having previously observed a reduced T lymphocyte proliferation in response to anti CD3 stimulation, we investigated whether this lack of proliferation reflected a diminished activation status of the T cells. We therefore examined the expression of the activation marker CD25. Increasing GO concentrations, starting from 1 %, led to a significant decrease in CD25 expression, indicating impaired T cell activation (Fig. 4B).

We observed similar trends when we assessed the effect of GO on T regulatory cells (Fig. 4C–D). While no effects were observed in unstimulated PBMCs (Fig. 4C), notable differences were evident in anti-CD3 stimulated PBMCs (Fig. 4D). Indeed, the two highest GO concentrations used (2 % and 5 %) reduced the polarization of CD4+ cells toward the Treg subset (Fig. 4D). Finally, for all investigated subsets, we found that the PLGA scaffold was well-tolerated and did not result in significant differences compared to the control condition.

3.5. High concentrations of graphene oxide adversely affect the viability of monocytes induced to differentiate into M2 macrophages

To evaluate the effect of GO on innate immunity, we co-cultured human monocytes induced to differentiate toward antigen presenting cells (M1 and M2 macrophages, mDC) with increasing concentrations of GO. First, we observed that the PLGA scaffold alone did not significantly affect the viability of the various monocytic-derived populations. Similarly, our findings indicate that GO does not significantly impact the viability of resting monocytes (Fig. 5). However, when monocytes are induced to differentiate into pro-inflammatory M1 macrophages or immunoregulatory M2 macrophages, we observed a reduction in cell viability that correlates with increasing GO concentrations. This effect reached statistical significance in the case of monocytes differentiated into M2 macrophages, particularly at the two highest GO concentrations tested (PLGA-GO2% and PLGA-GO5%). Finally, no significant differences were observed in the cell viability when monocytes were induced to differentiate into mature dendritic cells (mDCs), regardless of the GO concentration tested.

3.6. Graphene oxide (GO) impacts the ability of monocyte to differentiate toward antigen presenting cells

We then investigated the effect of GO on monocyte polarization toward antigen presenting cells. As previously reported, the PLGA scaffold alone did not induce significant changes compared to the control for all immune populations studied, including monocytes, M1 macrophages, M2 macrophages, and mDCs. Moreover, we observed that, similar to what was previously observed for CD4 lymphocytes, GO does not affect monocyte differentiation in the absence of stimulation (Fig. 6A). Solely an intermediate concentration of GO reduced the expression of the co-stimulatory molecule CD86. However, when monocytes were induced to differentiate into M1 or M2 macrophages, we observed notable differences directly correlated with the concentrations of GO to which the monocytes were exposed. In the context of M1 differentiation, high concentrations of GO led to a reduction in the expression of the differentiation marker CD197 (Fig. 6B). The most pronounced effects were observed during differentiation into M2 macrophages (Fig. 6C). At GO concentrations exceeding 1 %, there was a notable decrease in the expression of CD14, a marker typically associated with M2 macrophages. More significantly, there was a marked reduction in CD163, a well-established marker for M2 macrophages, as well as CD209 (Fig. 6C).

Interestingly, no differences were observed in the expression of the investigated markers during monocyte differentiation into mature dendritic cells (mDCs) (Fig. 6D). In this case, regardless of the GO concentration analyzed, no variations were detected in the levels of marker expressions (Fig. 6D).

4. Discussion

Graphene oxide (GO) has garnered significant interest due to its wide-ranging applications in various fields, including medicine [36]. Despite its potential, the impact of GO on the human immune system remains an area with limited understanding. This study aimed to investigate how GO, when embedded in the biocompatible PLGA biomaterial, could influence the viability and polarization of human peripheral blood mononuclear cells (PBMCs) and potentially affect the viability and differentiation of different immune cell populations.

The selection of PLGA as a biomaterial is based on its excellent biocompatibility and its low inflammatory activity [12,13]. This material is readily degraded by esterases and is efficiently cleared from the body through metabolic waste products [14,15]. Additionally, there are no reports of polymer accumulation in human organs when PLGA is used at low concentrations [16]. Furthermore, PLGA has been observed to induce only a minimal inflammatory response and display immunosuppressive effects [17–19]. Conversely, other studies have indicated that exposure to PLGA, whether in micro- or nanoparticle form, can lead to increased levels of IL-1β and TNFα in murine macrophages, suggesting that the release of inflammatory cytokines is size-dependent *[37]*.

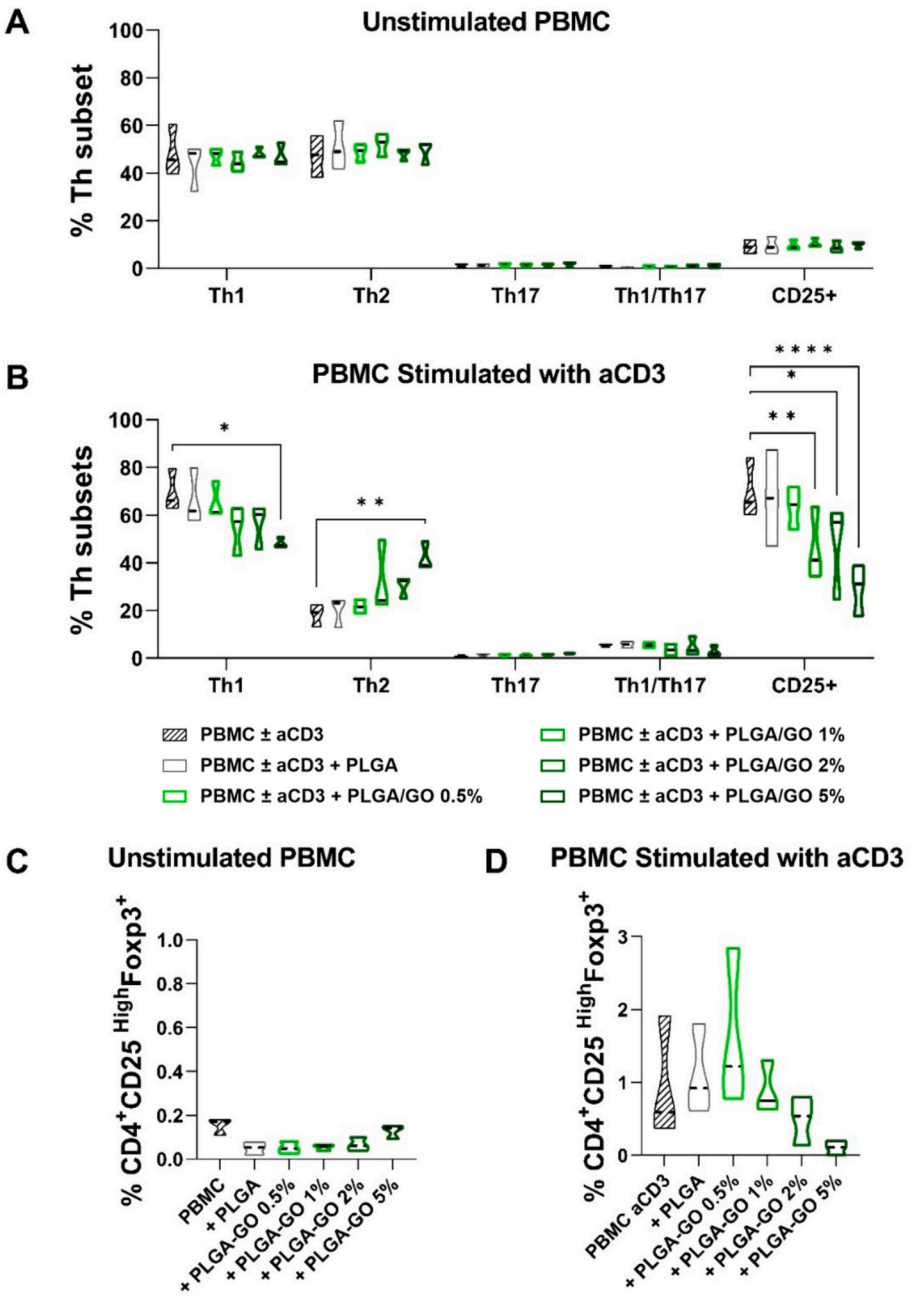

Fig. 4. Increasing concentrations of GO embedded in a PLGA matrix impact the differentiation of CD4+ T lymphocytes after stimulation with anti-CD3 monoclonal antibodies (mAbs). Unstimulated PBMC (A) or PBMC stimulated with anti-CD3 mAb (aCD3) (B) in the presence of PLGA scaffolds with different concentrations of graphene oxide (0.5, 1, 2 and 5 %) (GO) in comparison to the control condition in red, were harvested after six days of culture and analyzed for their polarization toward different Th subsets (Th1 (CD183 + CD196−), Th1/Th17 (CD183 + CD196+) and Th2 (CD183-CD196-CD194+), Th1/Th17 (CD183 + CD196+) and Th17 (CD183-CD196+)). Furthermore, the expression of the T lymphocyte activation marker CD25 was assessed (A–B). Induction of Treg was evaluated by flow cytometry six days after activation with anti-CD3 mAb and are displayed as a percentage of CD45RA − FoxP3 + CD25hi cells in unstimulated PBMC (C) and PBMC stimulated with aCD3 (D). Results are represented as violin plots showing median (thick line), 25th and 75th quartiles (*$p < 0.05$, **$p < 0.01$, ****$p < 0.0001$ versus control PBMC + antiCD3), $N = 3$ individual experiments. The data passed the Shapiro–Wilk test and the Kolmogorov–Smirnov normality test, thus exhibiting a normal distribution.

Another study noted that PLGA has the capacity to induce dendritic cell maturation toward an inflammatory phenotype [38]. Our findings are consistent with the literature reporting a lack of toxic or immunogenic effects of PLGA on immune cells. Specifically, we observed that PBMCs exposed solely to the PLGA scaffold did not exhibit any immunogenic response. The scaffold did not induce a pro-inflammatory response or alter the differentiation of T lymphocytes, macrophages, or dendritic cells, thereby supporting the use of PLGA as an embedding strategy for GO.

Furthermore, our study found that while increasing concentrations of GO did not affect unstimulated PBMCs and monocytes, significant changes were observed following cell stimulation. Specifically, exposure to high concentrations of GO progressively impaired viability and the activation and differentiation ability of stimulated T lymphocytes. The negative impact on activation was further evidenced by a marked reduction in the expression of the activation marker CD25, which is typically expressed 48 h post-stimulation [39,40]. This reduction, combined with the observed decrease in proliferation, indicates either a

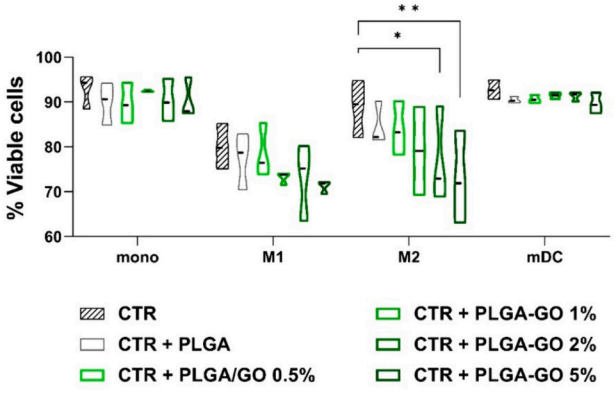

Fig. 5. Increasing concentrations of GO embedded in a PLGA matrix impact the viability of monocytes or monocytes differentiated toward antigen presenting cells. Unstimulated monocyte or monocytes stimulated with GM-CSF + LPS + IFNy (M1 macrophages), M-CSF + LPS + TNFa (M2 macrophages) or GM-CSF- + IL-4 + LPS (mDC), in the presence of PLGA scaffolds with different concentrations of graphene oxide (0.5, 1, 2 and 5 %) (GO) in comparison to the control condition in red, were harvested after six days in order to evaluate the ability to affect viability of monocytes alone or monocytes induced to differentiate toward M1 or M2 macrophages or mature dendritic cells (mDCs). Results are presented as a percentage of expression and are shown violin plots show median (thick line), 25th and 75th quartiles (*$p < 0.05$, ***$p < 0.001$, ****$p < 0.0001$ versus control), $N = 3$ individual experiments. The data passed the Shapiro–Wilk normality test, thus exhibiting a normal distribution.

failure in activation or a diminished capacity of T lymphocytes to respond to the activating stimulus.

Interestingly, the minimal effect on cell viability suggests that GO embedded within PLGA scaffolds may significantly impede T lymphocyte activation, potentially by disrupting metabolic processes [41].

In addition, the effects of GO were not limited to a reduced capacity of CD4+ T lymphocytes to differentiate into pro-inflammatory Th subsets, but also extended to the immunoregulatory CD4+ Treg subset.

Indeed, the reduction in IL-2 receptor expression can lead to a decrease in mTOR stimulation, thereby impacting the complete activation and differentiation of T lymphocytes. One group has demonstrated that IL-2–IL2R signaling plays a significant role in the differentiation of effector T cells. This process involves the downregulation of the transcription factor Kruppel-like factor 2 (KLF2), which governs the expression of critical homing molecules such as SP1, CD62L, CCR7, and various chemokine receptors. The authors reported that downregulation of KLF2 is contingent upon the activation of PI3K and entails the activation of mTOR [41]. In contrast, these findings deviated from other findings that report a significant stimulation of Th1/Th2 cytokine secretion by free GO nanoparticles suggesting increased T cell differentiation toward these subsets [42]. The embedded nature of GO within the PLGA matrix in this study could explain this difference, as it reduces direct cell contact.

Similar results were obtained when we analyzed the effects of GO on innate immunity. More in detail, increasing concentrations of GO did not affect the viability of resting monocytes; however, there was a concentration-dependent toxic effect when monocytes were induced to differentiate into pro-inflammatory M1 macrophages or anti-inflammatory M2 macrophages. Our results, obtained from primary cells derived from healthy donors, align with findings from studies using cell lines. Indeed, the consistent cytotoxic effects observed on macrophages are consistent with previous reports involving macrophage cell lines, such as human THP-1 and RAW 264.7 cells [43]. However, it should be emphasized that while the toxic effects on cell lines began to be significantly evident at a concentration of 100 μg/mL [43], in the case of the primary cells we employed, toxic effect were observed starting from 5 μg/mL, which corresponds to the highest concentration of GO

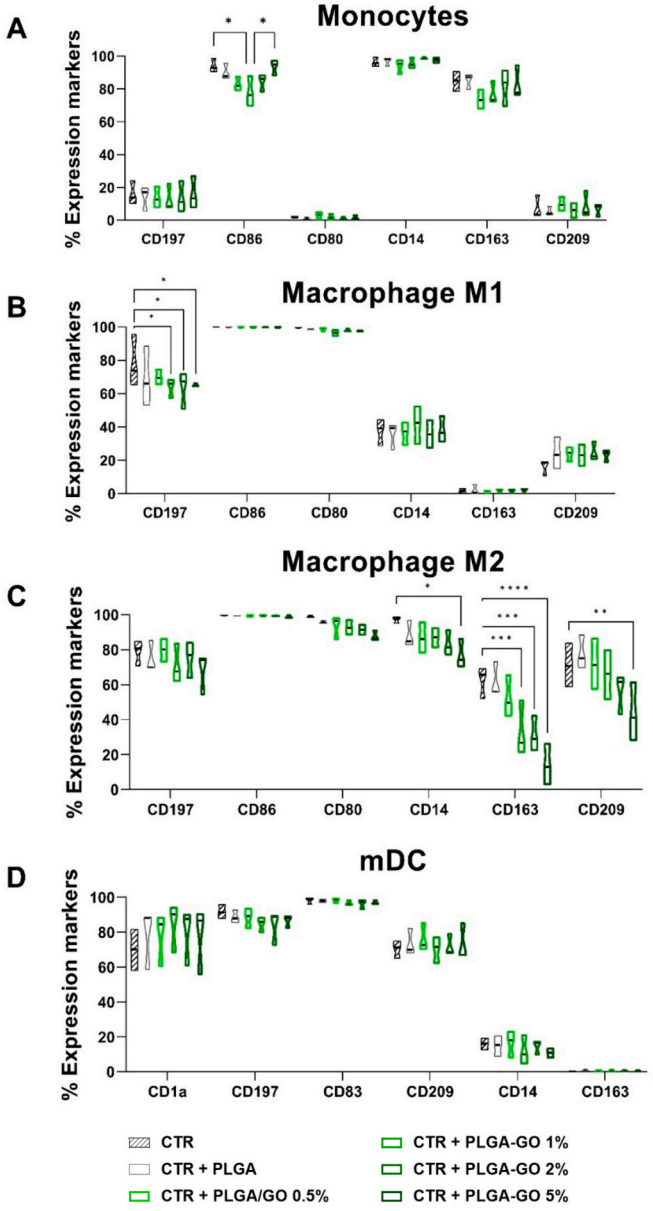

Fig. 6. Increasing concentrations of GO embedded in a PLGA matrix impact the differentiation of monocytes toward antigen presenting cells. Phenotype analysis of PBMC differentiated (panels B, C, D) or not (panel A) into macrophages (M1: panel B and M2: panel C) or into dendritic cells (DCs, panel D) in the presence of PLGA scaffolds at different concentration of graphene oxide (GO, 0.5, 1, 2 and 5 %) in comparison to the control condition in red (PLGA without GO). Scaffolds were added at the start of the differentiation protocol to evaluate the ability to affect monocyte differentiation toward M1 or M2 macrophages or mature DCs (mDCs). At the end of the culture period, expression of CD14, CD1a, CD209, CD197 and CD163 and of the co-stimulatory molecule CD80 and CD86 (CD83 instead of CD80 and CD86 for DCs) was evaluated by flow cytometry. Results are presented as a percentage of expression and are shown violin plots show median (thick line), 25th and 75th quartiles (*$p < 0.05$, ***$p < 0.001$, ****$p < 0.0001$ versus control), $N = 3$ individual experiments. The data passed the Shapiro–Wilk test and the Kolmogorov–Smirnov normality test, thus exhibiting a normal distribution for the plot A and B. For plot C the data passed the D'Agostino-Pearson omnibus K2 test.

tested in our study. In this sense, primary cells provide a more accurate and relevant model for studying toxicological effects, ultimately leading to better understanding and prediction of human health outcomes.

Other research has demonstrated that high concentrations of GO nanoparticles induce cytotoxicity in RAW cells, corroborating

observations related to pristine graphene [44]. Notably, GO has been shown to trigger mitochondrial membrane potential (MMP) depletion and an increase in intracellular ROS, leading to apoptosis via the mitochondrial pathway [44].

Moreover, GO nanosheets, following cellular internalization, can localize to F-actin filaments, causing alterations in the cell cycle and inducing apoptosis and oxidative stress. This effect was documented in both immune cells (RAW-264.7) and bone tissue-derived cells (Saos-2, MC3T3-E1 preosteoblasts) [45]. Another study reported that single-layer graphene reduces cell viability in A549 lung carcinoma cells and macrophage-like RAW264.7 cells by forming pores in the plasma membrane, ultimately resulting in cellular death [46]. Additionally, GO, when reduced with various biomolecules, exhibited increased cytotoxicity compared to non-reduced GO in both cancerous and non-cancerous cell types [47]. This heightened cell death associated with GO was linked to its hydrophilic properties, which facilitate cellular uptake compared to the hydrophobic reduced GO (rGO) [47].

As previously reported for resting T lymphocytes, GO did not induce negative effects on resting monocytes. Similarly, analysis of canonical markers revealed no impact on the expression of CD14 or CD80 in unstimulated monocytes, irrespective of the GO concentration examined. The detrimental effects of GO were observed when monocytes were induced to differentiate into M1 macrophages, with increasing GO concentrations leading to a reduction in the differentiation marker CD197, which is involved in macrophage recruitment [48]. Surprisingly, the most significant effects were observed during the differentiation of monocytes into immunoregulatory M2-like macrophages, where higher GO concentrations decreased CD14 expression and downregulated CD163 and CD209, markers typically associated with M2-like macrophages [49,50].

This observed effect may be attributed to GO's impact on monocyte viability during differentiation. Supporting this hypothesis, our results on the differentiation of monocytes into mature dendritic cells (DCs) showed no toxic effects from exposure to increasing GO concentrations. This absence of impact on DC differentiation markers reflects a lack of concentration-dependent variation. This outcome contrasts with other studies that reported GO-mediated inhibition of DC differentiation, primarily due to reduced co-stimulatory molecule CD83 levels [51]. In our study, this effect may have been mitigated by the incorporation of GO within the PLGA matrix.

5. Conclusion

Incorporating graphene oxide (GO) into polymers like PLGA enhances their stability in physiological conditions and mitigates immunological reactions. Our findings demonstrate that while GO in PLGA doesn't notably affect the viability of unstimulated PBMCs, it impedes the differentiation of T lymphocytes, especially at high concentrations. This underscores the necessity for precise optimization of biomaterials to prevent compromising immune function. Interestingly, GO incorporation minimally affects monocytes but significantly reduces the viability of M1 and M2 macrophages, impacting their differentiation toward M2-like macrophages. The observed discrepancy from previous studies on free GO nanoparticles may be attributed to the reduced cellular interaction provided by the PLGA matrix.

Although this is an in vitro study and lacks complementary in vivo research, our study stands out from most similar studies in the literature by examining the effects of PLGA-GO scaffolds on PBMCs isolated from healthy donors rather than using tumor-derived or immortalized cell lines, thereby offering enhanced physiological relevance.

Our findings indicate that while PLGA can attenuate immune-related adverse effects at elevated GO concentrations, caution is warranted due to the potential for these concentrations to significantly impair immune functionality. Given the prospective applications of PLGA-GO nanoparticles in drug delivery and thermotherapy, a comprehensive risk assessment is imperative to fully understand their potential impact on human health.

Funding information

This research was financially supported by the Ministero della Salute and the Italian Ministry of Research and University (MIUR, 5x1000, PRIN 2017 grant no. 2017RSAFK7), AIRC under the IG 2019—ID. 23124 project, (MP) and the Contributi per il finanziamento degli Enti privati che svolgono attività di ricerca - C.E.P.R. (2020−2022). Additionally, the Università Cattolica del Sacro Cuore provided funding for this research project and its publication through Linea D1 (OP).

CRediT authorship contribution statement

Andrea Papait: Writing – review & editing, Writing – original draft, Validation, Methodology, Investigation, Formal analysis, Data curation. **Giordano Perini:** Writing – review & editing, Writing – original draft, Methodology, Investigation, Formal analysis, Data curation. **Valentina Palmieri:** Writing – review & editing, Writing – original draft, Supervision. **Elsa Vertua:** Methodology, Investigation. **Anna Pasotti:** Methodology, Investigation. **Enrico Rosa:** Methodology, Investigation. **Marco De Spirito:** Writing – review & editing, Writing – original draft, Supervision. **Antonietta Rosa Silini:** Writing – review & editing, Writing – original draft. **Massimiliano Papi:** Writing – review & editing, Writing – original draft, Supervision, Funding acquisition, Conceptualization. **Ornella Parolini:** Writing – review & editing, Supervision, Funding acquisition, Conceptualization.

Declaration of competing interest

The authors declare that they have no known competing financial interests or personal relationships that could have appeared to influence the work reported in this paper.

Data availability

Data will be made available on request.

Acknowledgment

We would like to express our gratitude to the 3D Bioprinting Research Core Facility G-STeP and Microscopy Core Facility G-STeP of the Fondazione Policlinico Universitario “A. Gemelli” IRCCS for their contributions to sample processing.

References

[1] J. Li, H. Zeng, Z. Zeng, Y. Zeng, T. Xie, Promising graphene-based nanomaterials and their biomedical applications and potential risks: a comprehensive review, ACS Biomater Sci. Eng. 7 (12) (2021) 5363–5396.
[2] Z. Liu, J.T. Robinson, X. Sun, H. Dai, PEGylated nanographene oxide for delivery of water-insoluble cancer drugs, J. Am. Chem. Soc. 130 (33) (2008) 10876–10877.
[3] S. Liu, X. Pan, H. Liu, Two-dimensional nanomaterials for Photothermal therapy, Angew. Chem. Int. Ed. Engl. 59 (15) (2020) 5890–5900.
[4] R. Rauti, N. Lozano, V. León, D. Scaini, M. Musto, I. Rago, F.P. Ulloa Severino, A. Fabbro, L. Casalis, E. Vázquez, K. Kostarelos, M. Prato, L. Ballerini, Graphene oxide Nanosheets reshape synaptic function in cultured brain networks, ACS Nano 10 (4) (2016) 4459–4471.
[5] J.B. Shim, R.F. Ankeny, H. Kim, R.M. Nerem, G. Khang, A study of a three-dimensional PLGA sponge containing natural polymers co-cultured with endothelial and mesenchymal stem cells as a tissue engineering scaffold, Biomed. Mater. 9 (4) (2014) 045015.
[6] J.F. Mano, R.A. Sousa, L.F. Boesel, N.M. Neves, R.L. Reis, Bioinert, biodegradable and injectable polymeric matrix composites for hard tissue replacement: state of the art and recent developments, Compos. Sci. Technol. 64 (6) (2004) 789–817.
[7] H.R. Lin, C.J. Kuo, C.Y. Yang, S.Y. Shaw, Y.J. Wu, Preparation of macroporous biodegradable PLGA scaffolds for cell attachment with the use of mixed salts as porogen additives, J. Biomed. Mater. Res. 63 (3) (2002) 271–279.
[8] P. Gentile, V. Chiono, I. Carmagnola, P.V. Hatton, An overview of poly(lactic-co-glycolic) acid (PLGA)-based biomaterials for bone tissue engineering, Int. J. Mol. Sci. 15 (3) (2014) 3640–3659.

[9] L. Leung, C. Chan, S. Baek, H. Naguib, Comparison of morphology and mechanical properties of PLGA bioscaffolds, Biomed. Mater. 3 (2) (2008) 025006.
[10] C.V. Rocha, V. Gonçalves, M.C. da Silva, M. Bañobre-López, J. Gallo, PLGA-based composites for various biomedical applications, Int. J. Mol. Sci. 23 (4) (2022).
[11] A.N. Ford Versypt, D.W. Pack, R.D. Braatz, Mathematical modeling of drug delivery from autocatalytically degradable PLGA microspheres–a review, J. Control. Release 165(1) (2013) 29–37.
[12] M. Mir, N. Ahmed, A.U. Rehman, Recent applications of PLGA based nanostructures in drug delivery, Colloids Surf. B Biointerfaces 159 (2017) 217–231.
[13] K.A. Athanasiou, G.G. Niederauer, C.M. Agrawal, Sterilization, toxicity, biocompatibility and clinical applications of polylactic acid/polyglycolic acid copolymers, Biomaterials 17 (2) (1996) 93–102.
[14] R.P. Félix Lanao, S.C. Leeuwenburgh, J.G. Wolke, J.A. Jansen, In vitro degradation rate of apatitic calcium phosphate cement with incorporated PLGA microspheres, Acta Biomater. 7 (9) (2011) 3459–3468.
[15] E.M. Elmowafy, M. Tiboni, M.E. Soliman, Biocompatibility, biodegradation and biomedical applications of poly(lactic acid)/poly(lactic-co-glycolic acid) micro and nanoparticles, J. Pharm. Investig. 49 (4) (2019) 347–380.
[16] Y. Ramot, D. Touitou, G. Levin, D.E. Ickowicz, M.H. Zada, R. Abbas, L. Yankelson, A.J. Domb, A. Nyska, Interspecies differences in reaction to a biodegradable subcutaneous tissue filler: severe inflammatory granulomatous reaction in the Sinclair minipig, Toxicol. Pathol. 43 (2) (2015) 267–271.
[17] Y. Waeckerle-Men, E. Scandella, E. Uetz-Von Allmen, B. Ludewig, S. Gillessen, H. P. Merkle, B. Gander, M. Groettrup, Phenotype and functional analysis of human monocyte-derived dendritic cells loaded with biodegradable poly(lactide-co-glycolide) microspheres for immunotherapy, J. Immunol. Methods 287 (1–2) (2004) 109–124.
[18] J.S. Lewis, C. Roche, Y. Zhang, T.M. Brusko, C.H. Wasserfall, M. Atkinson, M. J. Clare-Salzler, B.G. Keselowsky, Combinatorial delivery of immunosuppressive factors to dendritic cells using dual-sized microspheres, J. Mater. Chem. B 2 (17) (2014) 2562–2574.
[19] R.P. Allen, A. Bolandparvaz, J.A. Ma, V.A. Manickam, J.S. Lewis, Latent, immunosuppressive nature of poly(lactic-co-glycolic acid) microparticles, ACS Biomater Sci. Eng. 4 (3) (2018) 900–918.
[20] C. Farrera, B. Fadeel, It takes two to tango: understanding the interactions between engineered nanomaterials and the immune system, Eur. J. Pharm. Biopharm. 95 (Pt A) (2015) 3–12.
[21] I. Dudek, M. Skoda, A. Jarosz, D. Szukiewicz, The molecular influence of graphene and graphene oxide on the immune system under in vitro and in vivo conditions, Arch. Immunol. Ther. Exp. (Warsz.) 64 (3) (2016) 195–215.
[22] G. Qu, S. Liu, S. Zhang, L. Wang, X. Wang, B. Sun, N. Yin, X. Gao, T. Xia, J.J. Chen, G.B. Jiang, Graphene oxide induces toll-like receptor 4 (TLR4)-dependent necrosis in macrophages, ACS Nano 7 (7) (2013) 5732–5745.
[23] S. Huang, S. Li, Y. Liu, B. Ghalandari, L. Hao, C. Huang, W. Su, Y. Ke, D. Cui, X. Zhi, X. Ding, Encountering and wrestling: neutrophils recognize and defensively degrade graphene oxide, Adv. Healthc. Mater. 11 (8) (2022) e2102439.
[24] S.P. Mukherjee, B. Lazzaretto, K. Hultenby, L. Newman, A.F. Rodrigues, N. Lozano, K. Kostarelos, P. Malmberg, B. Fadeel, Graphene oxide elicits membrane lipid changes and neutrophil extracellular trap formation, Chem 4 (2) (2018) 334–358.
[25] L. Xu, J. Xiang, Y. Liu, J. Xu, Y. Luo, L. Feng, Z. Liu, R. Peng, Functionalized graphene oxide serves as a novel vaccine nano-adjuvant for robust stimulation of cellular immunity, Nanoscale 8 (6) (2016) 3785–3795.
[26] A.V. Tkach, N. Yanamala, S. Stanley, M.R. Shurin, G.V. Shurin, E.R. Kisin, A. R. Murray, S. Pareso, T. Khaliullin, G.P. Kotchey, V. Castranova, S. Mathur, B. Fadeel, A. Star, V.E. Kagan, A.A. Shvedova, Graphene oxide, but not fullerenes, targets immunoproteasomes and suppresses antigen presentation by dendritic cells, Small 9 (9–10) (2013) 1686–1690.
[27] G. Perini, G. Ciasca, E. Minelli, M. Papi, V. Palmieri, G. Maulucci, M. Nardini, V. Latina, V. Corsetti, F. Florenzano, P. Calissano, M. De Spirito, G. Amadoro, Dynamic structural determinants underlie the neurotoxicity of the N-terminal tau 26-44 peptide in Alzheimer's disease and other human tauopathies, Int. J. Biol. Macromol. 141 (2019) 278–289.
[28] A.R. Silini, A. Papait, A. Cargnoni, E. Vertua, P. Romele, P. Bonassi Signoroni, M. Magatti, S. De Munari, A. Masserdotti, A. Pasotti, S. Rota Nodari, G. Pagani, M. Bignardi, O. Parolini, CM from intact hAM: an easily obtained product with relevant implications for translation in regenerative medicine, Stem Cell Res Ther 12 (1) (2021) 540.
[29] G. Friggeri, I. Moretti, F. Amato, A.G. Marrani, F. Sciandra, S.G. Colombarolli, A. Vitali, S. Viscuso, A. Augello, L. Cui, G. Perini, M. De Spirito, M. Papi, V. Palmieri, Multifunctional scaffolds for biomedical applications: crafting versatile solutions with polycaprolactone enriched by graphene oxide, APL Bioeng 8 (1) (2024) 016115.
[30] V. Palmieri, E.A. Dalchiele, G. Perini, A. Motta, M. De Spirito, R. Zanoni, A. G. Marrani, M. Papi, Biocompatible N-acetyl cysteine reduces graphene oxide and persists at the surface as a green radical scavenger, Chem. Commun. (Camb.) 55 (29) (2019) 4186–4189.
[31] A.G. Marrani, A. Motta, V. Palmieri, G. Perini, M. Papi, E.A. Dalchiele, R. Schrebler, R. Zanoni, A comparative experimental and theoretical study of the mechanism of graphene oxide mild reduction by ascorbic acid and N-acetyl cysteine for biomedical applications, Materials Advances 1 (8) (2020) 2745–2754.
[32] V. Palmieri, G. Perini, M. De Spirito, M. Papi, Graphene oxide touches blood: in vivo interactions of bio-coronated 2D materials, Nanoscale Horizons 4 (2) (2019) 273–290.
[33] T. Arasoglu, S. Derman, B. Mansuroglu, Comparative evaluation of antibacterial activity of caffeic acid phenethyl ester and PLGA nanoparticle formulation by different methods, Nanotechnology 27 (2) (2016) 025103.
[34] A.G. Marrani, R. Zanoni, R. Schrebler, E.A. Dalchiele, Toward graphene/silicon Interface via controlled electrochemical reduction of graphene oxide, J. Phys. Chem. C 121 (10) (2017) 5675–5683.
[35] G. Perini, V. Palmieri, A. Papait, A. Augello, D. Fioretti, S. Iurescia, M. Rinaldi, E. Vertua, A. Silini, R. Torelli, A. Carlino, T. Musarra, M. Sanguinetti, O. Parolini, M. De Spirito, M. Papi, Slow and steady wins the race: fractionated near-infrared treatment empowered by graphene-enhanced 3D scaffolds for precision oncology, Mater Today Bio 25 (2024) 100986.
[36] S. Priyadarsini, S. Mohanty, S. Mukherjee, S. Basu, M. Mishra, Graphene and graphene oxide as nanomaterials for medicine and biology application, J. Nanostructure Chem. 8 (2) (2018) 123–137.
[37] R. Nicolete, D.F. dos Santos, L.H. Faccioli, The uptake of PLGA micro or nanoparticles by macrophages provokes distinct in vitro inflammatory response, Int. Immunopharmacol. 11 (10) (2011) 1557–1563.
[38] M. Yoshida, J.E. Babensee, Differential effects of agarose and poly(lactic-co-glycolic acid) on dendritic cell maturation, J. Biomed. Mater. Res. A 79 (2) (2006) 393–408.
[39] A. Papait, A.R. Silini, M. Gazouli, R. Malvicini, M. Muraca, L. O'Driscoll, N. Pacienza, W.S. Toh, G. Yannarelli, P. Ponsaerts, O. Parolini, G. Eissner, M. Pozzobon, S.K. Lim, B. Giebel, Perinatal derivatives: how to best validate their immunomodulatory functions, Front. Bioeng. Biotechnol. 10 (2022) 981061.
[40] C. Poloni, C. Schonhofer, S. Ivison, M.K. Levings, T.S. Steiner, L. Cook, T-cell activation-induced marker assays in health and disease, Immunol. Cell Biol. 101 (6) (2023) 491–503.
[41] L.V. Sinclair, D. Finlay, C. Feijoo, G.H. Cornish, A. Gray, A. Ager, K. Okkenhaug, T. J. Hagenbeek, H. Spits, D.A. Cantrell, Phosphatidylinositol-3-OH kinase and nutrient-sensing mTOR pathways control T lymphocyte trafficking, Nat. Immunol. 9 (5) (2008) 513–521.
[42] H. Zhou, K. Zhao, W. Li, N. Yang, Y. Liu, C. Chen, T. Wei, The interactions between pristine graphene and macrophages and the production of cytokines/chemokines via TLR- and NF-κB-related signaling pathways, Biomaterials 33 (29) (2012) 6933–6942.
[43] Ó. Cebadero-Dominguez, A. Casas-Rodríguez, M. Puerto, A.M. Cameán, A. Jos, In vitro safety assessment of reduced graphene oxide in human monocytes and T cells, Environ. Res. 232 (2023) 116356.
[44] Y. Li, Y. Liu, Y. Fu, T. Wei, L. Le Guyader, G. Gao, R.S. Liu, Y.Z. Chang, C. Chen, The triggering of apoptosis in macrophages by pristine graphene through the MAPK and TGF-beta signaling pathways, Biomaterials 33 (2) (2012) 402–411.
[45] M.C. Matesanz, M. Vila, M.J. Feito, J. Linares, G. Gonçalves, M. Vallet-Regi, P. A. Marques, M.T. Portolés, The effects of graphene oxide nanosheets localized on F-actin filaments on cell-cycle alterations, Biomaterials 34 (5) (2013) 1562–1569.
[46] G. Duan, Y. Zhang, B. Luan, J.K. Weber, R.W. Zhou, Z. Yang, L. Zhao, J. Xu, J. Luo, R. Zhou, Graphene-induced pore formation on cell membranes, Sci. Rep. 7 (2017) 42767.
[47] S. Gurunathan, M.H. Kang, M. Jeyaraj, J.H. Kim, Differential immunomodulatory effect of graphene oxide and vanillin-functionalized graphene oxide nanoparticles in human acute Monocytic leukemia cell line (THP-1), Int. J. Mol. Sci. 20 (2) (2019).
[48] J. Liu, X. Geng, J. Hou, G. Wu, New insights into M1/M2 macrophages: key modulators in cancer progression, Cancer Cell Int. 21 (1) (2021) 389.
[49] Y. Wang, K. Yan, J. Wang, J. Lin, J. Bi, M2 macrophage co-expression factors correlate with immune phenotype and predict prognosis of bladder Cancer, Front. Oncol. 11 (2021) 609334.
[50] A. Papait, E. Ragni, A. Cargnoni, E. Vertua, P. Romele, A. Masserdotti, C. Perucca Orfei, P.B. Signoroni, M. Magatti, A.R. Silini, L. De Girolamo, O. Parolini, Comparison of EV-free fraction, EVs, and total secretome of amniotic mesenchymal stromal cells for their immunomodulatory potential: a translational perspective, Front. Immunol. 13 (2022) 960909.
[51] S.V. Uzhviyuk, M.S. Bochkova, V.P. Timganova, P.V. Khramtsov, K.Y. Shardina, M. D. Kropaneva, A.I. Nechaev, M.B. Raev, S.A. Zamorina, Interaction of human dendritic cells with graphene oxide nanoparticles in vitro, Bull. Exp. Biol. Med. 172 (5) (2022) 664–670.